Role of cations on the dissolution mechanism of kaolinite in high alkaline media

Noel Essey N'Guessan, Emmanuel Joussein, Alexandra Courtin-Nomade, Erwan Paineau, Marilyne Soubrand, Olivier Grauby, Valentin Robin, Coelho Diogo Cristina, Delphine Vantelon, Pascale Launois, et al.

Role of cations on the dissolution mechanism of kaolinite in high alkaline media

Noel Essey N'GUESSAN[1], Emmanuel JOUSSEIN[1*], Alexandra COURTIN-NOMADE[2], Erwan PAINEAU[3], Marilyne SOUBRAND[1], Olivier GRAUBY[4], Cristina COELHO DIOGO[5], Delphine VANTELON[6], Pascale LAUNOIS[3], Valentin ROBIN[1], Patrice FONDANECHE[1], Sylvie ROSSIGNOL[7], Nathalie TEXIER-MANDOKI[8], Xavier BOURBON[8]

[1] Université de Limoges, FST, E2Lim PEIRENE-EAU EA 7500, 123 avenue Albert Thomas, 87060 Limoges, France.

[2] Université Paris-Saclay, CNRS, GEOPS, Orsay, 91405, France.

[3] Université Paris-Saclay, CNRS, Laboratoire de Physique des Solides, Orsay, 91405, France

[4] Centre Interdisciplinaire de Nanoscience de Marseille (CINaM), CNRS/Aix-Marseille Université, Campus de Luminy, 13288 Marseille, France.

[5] Institut des Matériaux de Paris Centre FR2482, Sorbonne Université, Faculté des Sciences et Ingénierie, 4 place Jussieu 75005 Paris, France.

[6] Synchrotron SOLEIL, LUCIA beamline, L'Orme des Merisiers, 91190 Saint-Aubin, France.

[7] Université de Limoges, IRCER, Centre Européen de la Céramique, 12 rue Atlantis, 87068 Limoges, France.

[8] Andra, Agence Nationale pour la Gestion des Déchets Radioactifs, 92290 Châtenay-Malabry, France.

* Corresponding author. Emmanuel JOUSSEIN, Université de Limoges, FST, E2Lim PEIRENE-EAU EA 7500, 123 avenue Albert Thomas, 87060 Limoges, France. Mail. emmanuel.joussein@unilim.fr

To be submitted to Applied Clay Science

Abstract

Kaolinite and its dehydroxylated forms are widely used in industrial applications, particularly in alkaline media. Geopolymers are among the latest applications that are attracting significant interest. Until now, a deep understanding of the dissolution mechanism of kaolinite particles in alkaline media is still lacking. This work aims to well understand the dissolution mechanisms of two references kaolinites (KGa-1b and KGa-2) regarding various 2 M alkali treatment (KOH, NaOH and 50/50 NaOH + KOH) along time and at 80°C through aluminum and silicon leaching. For this, a wide range of methods have been used, from the determination of [Si] and [Al] in solution to the analysis of solids by combining X-ray diffraction (XRD), Fourier Transformed Infrared (FTIR), X-ray Absorption Near edge Structure (XANES) and Magic Angle Spinning Nuclear Magnetic Resonance (MAS-NMR) spectroscopies and electronic microscopy observations. The results show that the dissolution rate is higher in the poorly crystallized kaolinites (confirming the role of the crystallinity of the samples towards reactivity in an alkaline media) but also a significant effect of the type of cation (the degree of dissolution following the

43 sequence KOH<NaOH + KOH<NaOH). This dissolution is followed by a change in the
44 speciation of the aluminum from 6-coordinated to a 4-coordinated, as shown by XAS and MAS-
45 NMR results. The dissolution process at the particle scale is different: with KOH, the dissolution
46 is homogeneous, starting from the edges and surfaces, whereas in the case of NaOH, the
47 dissolution is oriented thanks to areas of less coherence.

48

49 **Highlights:**

50 • The degree of dissolution of kaolinites is linked to the type of alkaline treatment.
51 • The dissolution rate is higher in the poorly crystallized kaolinites.
52 • The dissolution is accompanied by a change in the speciation of the aluminum.
53 • The particle dissolution process is homogeneous in KOH and oriented with NaOH

54

55 **Keywords:** alkaline activation, kaolinite, XRD, TEM-EDS, XANES, MAS-NMR, dissolution.

56

57 **Graphical abstract:** see attached file

58

59 ## 1. Introduction

60 Since the past decades, there has been increasing interest in producing eco-friendly geomaterials
61 from natural and inexpensive materials such as alkali activated materials *s.l.* or specifically
62 geopolymers. These geomaterials are promising since their properties are comparable to that
63 obtained from Ordinary Portland Cement (OPC) while reducing the energy required during

manufacture (Habert et al., 2011). Geopolymers result from the activation of aluminosilicates sources, such as fly-ash or clay minerals used as precursors, in a high concentrated alkali media (NaOH or KOH) to form free SiO_4 and AlO_4 tetrahedrons at ambient temperatures. The polycondensation (*i.e*. geopolymerization reaction) results from the reaction of aluminate and silicate dissolved monomers (Duxson et al., 2007; van Deventer et al., 2007). The tetrahedrally coordinated aluminum carries a negative charge that is counterbalanced by an alkali cation such as Na^+ or K^+. Finally, geopolymers present an amorphous 3D aluminosilicate structure. It is widely accepted that the resulting properties of geopolymer binder depend on the Si/Al ratio of the initial mixture and the kinetic dissolution of the raw aluminosilicate source (i.e., rate and relative amount of Si and Al release in the solution; Catauro et al., 2014). Thus, understanding the chemical reactivity of the Si and Al source during the first steps of an alkali treatment is key to better predict, and control, the properties of geopolymer based materials.

The main source of aluminosilicates in this context is the kaolinite. Kaolinite is a dioctahedral 1:1 clay mineral highly used in a variety of industrial applications (*e.g.* paper-coating, filler, paint pigment, ceramics, pharmaceutical to cite a few; see large literature such as Murray (2006)). The theoretical formulae of kaolinite is $Al_2Si_2O_5(OH)_4$ in which one Al octahedral sheet and one Si tetrahedral sheet are linked to each other by sharing apical oxygen atoms from the tetrahedral sheet. One of the main characteristics of most varieties of kaolinite is a defective structure (Bailey, 1988; Brindley, 1986; Sakharov et al., 2016) resulting in a variety of physical and chemical properties governing its uses (Murray, 2000). Moreover, it is common to modify the properties of raw material in the way to increase their reactivity by thermal treatment or grinding for instance (San Nicolas et al., 2013). According to this, kaolinite is conventionally heat-treated to form metakaolin. The metakaolin is the most used material for geopolymers because of its initial Si and Al content (highest alumina content) but also because of its rapid dissolution in

alkaline medium which will confer various properties (such as mechanical properties, high fire resistance…) of use to geopolymers (Autef et al., 2013). The reactivity of metakaolin depends on several factors: (i) the dehydroxylation process of kaolinite as well as the applied temperature, i.e. flash calciner, rotary kiln or vertical multiple-hearth oven from 500 to 800 °C (Belver et al., 2002), (ii) the purity *i.e*. the amount of accessories minerals (up to 30% in mixture) such as quartz, feldspars, rutile or anatase (Cui et al., 2008; Medri et al., 2011), and (iii) the properties of the initial primary kaolinite crystals (Kuenzel et al., 2013; Rahier et al., 1997). The latter is an important factor depending on the type of deposit and is mainly related to the crystal chemistry of the initial kaolinite (Heller-Kallai and Lapides, 2007). However, the impact of the primary kaolinite crystal chemistry used for the metakaolin processing on their reactivity in alkaline media is still not clear. Therefore, it is essential to fully understand the main factors that drive the reactivity of kaolinites in an alkaline medium through the dissolution of its component species. The dissolution process of kaolinite under different conditions in terms of alkali type (NaOH or KOH), concentration, pH and temperature has been previously mentioned in the literature. For example, Huertas et al. (1999) studied the dissolution of kaolinite over a pH range of 1 to 13. The authors evidenced a deprotonation of the octahedral surface occurring at high pH value (> 9) along with the formation of an AlO^- type surface complex followed by the release of structural Al and the dissolution of kaolinite particles. Interestingly, the octahedral layer also appears to be the main factor limiting the dissolution rate of kaolinite in an alkaline solution (KOH of 0.1 to 4 M; Bauer and Berger (1998)). These findings agree with the previous work of Carroll and Walther (1990) which evidenced a slower detachment of Si from the kaolinite structure (thus forming SiO- complexes) than that of Al when the clay particles were dissolved. Pentrak et al. (2009) demonstrated, during an alkaline treatment in KOH, that a lower structural ordering and a less regular shape of the crystallites are causing faster dissolution. In terms of cationic effect (*e.g*.

112 Na^+, K^+…), it would suggest that the degree of dissolution of Al and Si atoms is significantly
113 higher (40%) in a sodium hydroxide (NaOH) solution than in a KOH solution[22]. Recently, Naderi
114 Khorshidi et al. (2017, 2018) have studied by molecular dynamics simulation, the modification
115 and/or dissolution of two basal surfaces of kaolinite in various alkaline media (1 M and 5 M) for
116 three different alkaline solutions (containing Na^+, K^+ and a mixture of 50/50 Na^+/K^+ cations) at
117 ambient conditions. The results evidence that Na^+ and K^+ induce different dissolution
118 mechanisms related to different dissociation of the surface hydroxyl groups of kaolinite particles.
119 The authors also explained that a synergistic effect of both cations is effective in the case of the
120 50/50 mixture leading to more surface structure distortion.
121 Until now, a deep understanding of the dissolution mechanism of kaolinite particles is still
122 lacking. It requires considering both the crystallochemistry of kaolinite, the nature of cation
123 (containing Na^+, K^+ and a mixture of Na^+/K^+ cations) and their impact onto the solid structure. It
124 is essential to understand how kaolinite reacts (dissolves) in an alkaline medium in order to better
125 understand geopolymerization reactions (quantity of Si and Al species in solution, speciation of
126 Al *i.e.* (IV)- or (VI)-coordinated) and the choice of aluminosilicate mineral raw material. Here,
127 we proposed to better understand the dissolution mechanisms of two references kaolinites (KGa-
128 1b and KGa-2) regarding various 2 M alkali treatment (KOH, NaOH and 50/50 NaOH + KOH;
129 type of alkali solutions was chosen according to the geopolymerization literature; see for example
130 Aldabsheh et al. (2015) or Xu and van Deventer (2000)) along time and at 80°C through
131 aluminum and silicon leaching. These two references kaolinites, KGa-1b and KGa-2, differ in
132 terms of structural disorder. In this framework, we studied the release of both Al and Si from
133 kaolinite platelets by monitoring the structural evolution of the solid phase by combining X-ray
134 diffraction (XRD), Fourier Transformed Infrared (FTIR), X-ray Absorption Near edge Structure
135 (XANES) spectroscopies and microscopy observations. Altogether, our results unravel (i) the

136 importance of kaolinite crystallochemistry on its chemical reactivity, (ii) the effect of the type of
137 cation toward dissolution rates and associated mechanisms and then (iii) the occurrence and
138 effect on dissolution rates and solid modification of different dissolution mechanisms involved in
139 alkaline media treatments.
140

141 ## 2. Material and Methods

142 ### 2.1. Background onto reference kaolinites

143 Two reference kaolinites referred as KGa-1b and KGa-2 hereafter were provided by the Clay
144 Mineral Society. These kaolinites are representative of commonly occurring, natural kaolinite
145 materials and are distinguished by phase purity and availability (Sakharov et al., 2016). These
146 two samples are well known in the literature (for example reader referred to the baseline studies
147 of the Clay Minerals Society source clays in Costanzo and Guggenheim (2001)), the main
148 properties (chemical analysis and main physico-chemical properties) are reported in the Table SI
149 1 in Supplementary Information. The initial mineralogy is dominated by kaolinite (96 % for
150 KGa-1b and KGa-2) with some accessory minerals, i.e. 3% of anatase and 1% of quartz for KGa-
151 1b; 3% of anatase and 1% of mica and/or illite and quartz for KGa-2. The presence of other
152 silicate minerals than kaolinite, *e.g.* quartz, may imply a Si/Al ratio slightly different than 1 in
153 agreement with chemical analyses reported in Table SI 1.
154

155 ### 2.2. Alkali treatment experiment

156 The treatment was performed at 80°C in three different alkali media (pure KOH, pure NaOH, or a
157 mixture of KOH + NaOH 50/50) at the same 2 M concentration in OH (*ca* pH 14). Briefly, KOH

158 and NaOH pellets (VWR analytical reagents grade) were dissolved in double-deionized water.
159 300 mg of KGa-1b or KGa-2 were mixed with 30 ml of 2 M alkali solutions in Teflon vessels.
160 The mixtures were shaken in a Memmert water-bath stirrer at 80°C at various time steps (1, 3, 6,
161 12, 24 h). Each experiment was realized in sacrificial mode. After shaking, the liquid and the
162 solid phases were separated by centrifugation at 2734 g for 5 min at room temperature. The
163 supernatants were filtered at 0.45 µm from cellulose acetate filters and diluted in acidic media
164 (HNO_3 2%) prior to analysis. The solid residues were rapidly washed twice by dispersion in de-
165 ionized water and centrifugation at 4000 rpm for 5 min to stop alkali treatment and dried at 45°C
166 in an oven for structural and microscopic investigations. All the experiments were carried out in
167 duplicate.

168 The Si and Al chemical analyses were conducted on a microwave plasma-atomic emission
169 spectrometer (MP-AES, Agilent MP 4100) coupled with a high-performance liquid
170 chromatography (HPLC) setup, modified for analyzing strong alkali solutions. The measurement
171 errors were less than 10% based on reproducibility tests.

172 **2.3. Characterization of solid phases**

173 XRD was carried out on a Bruker D8 diffractometer operating with Cu Kα radiation (λ=0.154
174 nm). The samples were prepared as disoriented powders and scanned between 2 – 65 °2θ with a
175 0.02 °2θ step for 1 s per step. X'Pert Highscore software was used for qualitative identification of
176 minerals. The crystallinity index of each samples was estimated using the Hinckley index
177 according to Plançon et al. (1988); it is based on the ratio of the sum of the intensity of the $(1\bar{1}0)$
178 and $(1\bar{1}1)$ reflections measured from the inter-peak background, and the intensity of the $(1\bar{1}0)$
179 peak determined from the general background. FTIR spectroscopy was performed on a Perkin

Elmer spectrometer using attenuated total reflectance (ATR) in the middle infrared (MIR) region (4000 – 600 cm^{-1}) and each final spectrum is the average of 5 scans. The theoretical resolution of the device is 2 cm^{-1}. Omnic software was used for spectrum analyses.

Al and Si K-edges XANES experiments were undertaken at LUCIA beamline (Soleil synchrotron, France). The X-ray beam was monochromated using a pair of KTP (011) crystals. The energy was calibrated at the first inflexion point of the Al K-edge of an aluminum foil (1559 eV) or of a silicon foil for the Si-K-edge (1839 eV). Spectra were collected in steps of 2 eV below the edge, of 0.2 eV in the edge region and of 1 eV behind the edge, at a counting rate of 2 s per step. Data were recorded in fluorescence mode using a mono-element silicon drift diode detector and corrected for the detector dead time. Data processing, normalization and analysis were performed with the Athena software (Ravel and Newville, 2005). Data were corrected for self-absorption based on the theoretical chemical formula of the mineral phases contained in the samples. References used for (i) Al K-edge XANES were synthetic gibbsite ($Al(OH)_3$), synthetic kaolinite, boehmite (γ-AlO(OH)), orthoclase and andalusite (Figure SI 1 supplementary information), and for (ii) Si K-edge XANES, quartz, kaolinite, orthoclase, andalusite and halloysite (Figure SI 1 supplementary information).

Solid-state NMR experiments were performed on a Bruker AVANCE III 700 spectrometer at 16.4 T ($\nu_0(^{27}Al)$ = 182.47 MHz) with 2.5 mm (25 kHz) double resonance Bruker MAS probes and with samples spun at the magic angle using ZrO_2 rotors. For quantitative purposes, all 1D ^{27}Al (I = 5/2) MAS NMR spectra were obtained by using short pulses ($<\pi/8$). Nutation curves were first established by using a solution of 1M $Al(NO_3)_3$ ($t_{90°}(^{27}Al)$ = 3.2 µs, Recycle delay = 0.5s, number of scans = 6000-12000). 2D ^{27}Al 5QMAS NMR spectra (Medek et al., 1995) were obtained by using an amplitude modulated Z-filter experiment (p_1-t_1(5Q evolution)- p_2-τ-p_3-

t_2(acquire) (Amoureux et al., 1996). The optimized pulse lengths of the 5Q excitation (p_1) and reconversion (p_2) were p_1 = 4.5 µs and p_2 = 1.5 µs, respectively, implemented with an rf field of 55 and 165 kHz, whereas the soft π/2 Z-filter (p_3) was set to 6.5 µs, which was delivered with an rf field of ~40 kHz (recycle delay = 0.2s, number of scans = 6000). ^{27}Al NMR chemical shifts were referenced to a 1M solution of $Al(NO_3)_3$, respectively. All decompositions of spectra were performed using the DMfit software (Massiot et al., 2002), available free of charge online. For ^{27}Al spectra, previous studies have clearly demonstrated the combined role of quadrupolar interaction and CSA on the line shapes, especially at high magnetic field (Papulovskiy et al., 2013). Lorentz/ Gaussian (L/G) line shapes were used for AlIV sites end the int2QUAD DMfit module was used under the assumption of finite rotation frequency for the central transitions for AlVI sites. The following parameters were taken into account for each ^{27}Al sites: $\delta_{iso}(^{27}Al)$, $C_Q(^{27}Al)$, $\eta_Q(^{27}Al)$, d(CSA) corresponding to full Width at Half Maximum of the isotropic chemical shift *gaussian* distribution.

The morphology of samples was observed (a) by Scanning Electron Microscope (SEM) on a JEOL IT300 LV operating at 10kV, samples being previously carbon coated, and (b) by Transmission Electron Microscope (TEM) using a JEOL JEM 2011 (CiNAM). For TEM observations, samples were suspended in water and left to dry on gold and copper grids. The analyses were conducted at the accelerating voltage of 200 kV. The parameters were 50 000× magnification, 20° tilt angle toward the EDX detector, energy range of 40 keV, corrected counting time of 30 s, constant beam density ~63.5 pA.cm^{-2}. Elements were quantified using the Bruker AXS TEM line mark data semi-quantification procedure (Berthonneau et al., 2014). EDX chemical analyses were performed on 20 individual particles. The size of the particles (mean from 30 particles) was manually measured on micrographs using ImageJ software.

226

227 ## 3. Results and discussion

228 ### 3.1. Alkali dissolution kinetics of kaolinites samples

229 Figure 1 presents the evolution of Al and Si released during the dissolution of KGa-1b and KGa-
230 2 kaolinites with 2M alkali solutions at 80°C along time. The kinetic of dissolution of kaolinites
231 exhibits gradual release of [Al] and [Si] in solution whatever the type of kaolinites used until 12h
232 with 2M of KOH or KOH + NaOH, and following a log function as a function of time (t < 12h)
233 reflecting a decrease of the dissolution rate with time. However, the two kaolinites do not react
234 in the same way after 12h since in the case of KGa-2, it seems that there is a stabilization of the
235 dissolution which is not the case for KGa-1b except for a mixed alkaline treatment. The
236 dissolution phenomena observed by Bauer et al. (1998) on well-crystalline kaolinite at 80°C in
237 2M KOH evidenced that the change of slope occurs after 3-4 days when the concentrations of Si
238 and Al are greater than 7 mmol/l. In our case the reaction is faster with a clear change of slope
239 after 6hand Si and Al concentrations reaches values of 40 and 50 mmol/l for KGa-1b and KGa-2
240 respectively. A drastic decrease of [Al] and [Si] in solution is observed in the case of a NaOH
241 treatment after 6 h, this effect being more pronounced and very rapid in the case of KGa-2
242 compare to KGa-1b (12h). This feature can be attributed to a re-precipitation phenomenon of
243 solid(s) phase(s) that control concentration of Si and Al in solution (see discussions in section 3.2
244 Mineralogical evolution of kaolinite dissolution in high alkali media). Up to 6h, NaOH and KOH
245 + NaOH mixtures seem to be the most efficient for the dissolution of both kaolinites (about 75%
246 ± 2% of total Al and Si are released by KGa-1b and 82% ± 2% released by KGa-2). However,
247 after 6 hours, there is a secondary phase precipitation that results in a decrease of Si and Al
248 concentrations in solution. Note that such decrease in aqueous Si and Al concentrations does not

mean that the dissolution reaction of the kaolinite is limited, and the reverse may be the case with an increase of the kaolinite dissolution as the thermodynamic equilibrium may not be reach due to the involvement of aqueous Si and Al in a side reaction, *i.e.* precipitation of secondary phases. With KOH treatment, 60 to 70% (± 2%) of total Al and Si are released in solution from both kaolinites. The orders of efficiency of alkaline treatment for the kaolinite dissolution follows: KOH < KOH + NaOH ≤ NaOH, taking into consideration a duration up to 6h since the re-precipitation occurs after. The results relative to the main efficiency of NaOH are in accordance with others study on the dissolution of different industrial aluminosilicate minerals in similar alkali media (Panagiotopoulou et al., 2007; Xu and van Deventer, 2003). However, this contrasts with the results from molecular dynamic simulations of Naderi Khorshidi et al. (2018) that suggest the cation with low charge density K^+ encouraged more dissociation of the aluminate groups than the Na^+ one.

Si/Al molar ratio is calculated at each time step for all experiments, and the results show that the ratio is < 1 (0.80 < Si/Al < 0.98) regardless of the type of kaolinite at t < 6h, then stabilizes around 1 (0.99 ± 1) between 6 and 12 h for most of the experiments (Figure SI 2 Supplementary Information). Note that the Si/Al ratio of a theoretical kaolinite is closed to 1. To conclude, these data show that the rapid dissolution is incongruent at first during the alkaline attack and then becomes congruent over time.

3.2. Mineralogical evolution of kaolinite dissolution in high alkali media

3.2.1. XRD and FTIR measurements

X-ray diffractograms were acquired on both initial materials and the alkali treatment residues (Figure 2) to characterize any significant changes of the solid phase during the alkali treatment.

272 The two kaolinite samples differ essentially in terms of crystallinity, i.e. amount and nature of
273 structural defect. KGa-1b is a low-defect kaolinite (Hinckley index = 1.01) whereas KGa-2 is the
274 high-defect one (Hinckley index = 0.37). The effect of the crystallinity results in higher values of
275 CEC and SSA for KGa-2, the high defect one, compared to the KGa-1b. Two types of structural
276 disorder can be considered in KGa-1b and KGa-2: one for KGa-2 from random interstratification
277 of thin enantiomorphic blocks and a low ordered population of crystallites in which layer
278 displacements occur in relatively high proportions; a second one for KGa-1b, corresponding to
279 the highly ordered population of crystallites, due to structural periodicity seldom disturbed by
280 isolated stacking faults (Sakharov et al., 2016).

281 A significant decrease in post-treatment diffraction peaks is observed regardless of the type of
282 kaolinite and the type of reflections, *i.e*. basal (00l) or (hkl), indicating changes in the diffracting
283 domain size distribution and implying that the crystal shape changes. These results are in
284 accordance with those of Pentrak et al. (2009) who observed similar decreases of the diffraction
285 peaks along alkaline treatment with 4 M KOH solution. The alteration of the diffraction peaks is
286 in accordance with kinetic data that clearly evidences a dissolution of crystallites in an alkaline
287 medium. It results in a decrease over time of the Hinckley crystallinity index and a decrease in
288 the ratio of (060)/(001) reflection band which may be similar to a reduction in coherence in the *b*
289 direction of the kaolinite platelets. As expected, KGa-2 also shows a greater extent of dissolution,
290 i.e. alteration, probably due to the lower crystallinity, so the decrease is thus more pronounced.
291 Actually, it is not possible from XRD data to define the type of alteration and the mechanisms
292 involved. In the case of the sodium treatment (NaOH 2 M), XRD measurements also evidence the
293 presence of a new solid phase with several Bragg peaks corresponding to 6.34, 4.44, 3.64, and
294 2.56 Å inter-planar distances (Figure 2) related to a losod compound according to the JCPDS file

31-1269 (theoretical formulae $Na_{12}Al_{12}Si_{12}O_{48}$, 18 H_2O). This mineral phase is a polytype of hydroxysodalite and basically belonging to zeolite mineral group, explaining the decrease of the [Al] and [Si] in chemical analysis after 12h of contact time (Figure 1).

The zeolite precipitation is also pointed out by SEM observations (Figure SI 3 Supplementary information) and after by FTIR (Figure 3). The formation of zeolites particles, uniform in size and shape whatever the initial kaolinite sample, with the appearance of "wool ball" are noticeable for both kaolinites (KGa-1b and KGa-2, Figure SI 3). This is in accordance with the literature where several authors (*e.g.* Lin et al., 2004; Singer and Berkgaut, 1995) have obtained this type of zeolite in concentrated sodium alkaline medium (> 3.5 M NaOH) at room temperature. In our case, losod is obtained at a lower initial NaOH concentration because the reaction takes place at 80°C, which facilitates precipitation in lower concentrations. Sieber and Meier (1974) showed that zeolite-like losod crystallized only from mixtures with low sodium contents ($0.25 \leq Na/Al \leq 1$ and $Si/Al \leq 1$). In this experiment, the alkali treatment of kaolinite in NaOH leads to Na/Al = 0.63 and Si/Al = 1, confirming the possibility for zeolite to precipitate. Na^+ is then easily and rapidly recombined with Al and Si in solution leading to zeolite precipitation. Finally, the presence of zeolites-like or other phases resulting from precipitation in a basic medium was not observed in the case of KOH or NaOH + KOH. This means that the presence of K in the system inhibits the precipitation of zeolite under these experimental conditions. However, Bauer et al. (1998) have observed the precipitation of phillipsite-type zeolite in KOH 2M at 80°C but after 30 days of time contact of a kaolinite sample. This difference may be related for the authors to the presence of accessories minerals in the initial sample acting as precursors, which are not present in the KGa-1b and KGa-2 samples.

317 ATR-FTIR measurements in the MIR range are reported in Figure 3. The focus is previously
318 done on the case of KOH or KOH + NaOH treatments for 24 h. The data evidences (i) in the OH-
319 stretching region, a decrease of the ν1 band (3690 cm^{-1}) coupled with a slight decrease in
320 absorbance of the ν2 and ν3 bands located at 3669 and 3650 cm^{-1}. These three bands are
321 respectively due to the 3 inner surface hydroxyls. The ν1 and ν2 bands are the coupled
322 antisymmetric and symmetric vibrations (Brindley, 1986) whereas the ν3 is due to symmetry
323 reduction from an inner surface hydroxyl (Farmer and Russell, 1964). The fourth band ν4 at
324 about 3620 cm^{-1} is attributed to the inner hydroxyl (Johnston et al., 1990; Rouxhet et al., 1977);
325 (ii) in the Al-bending vibration range (δAl2-OH; 935 and 912 cm^{-1} corresponding to the OH of
326 inner-surface hydroxyl groups and the OH deformation of inner hydroxyl groups), no difference
327 is effective between spectra of both treated kaolinite; (iii) in the case of the absorption band near
328 1000 cm^{-1} related to a polymeric tetrahedral aluminosilicate network (Farmer et al., 1979), a
329 slight increase of the band located at 1005 cm^{-1} is observed along alkali treatment. It was reported
330 in the literature that this band can be relative to an excess of AlO_4 units in the aluminosilicate
331 framework (Pentrák et al., 2009). Finally, in highly alkaline solution (KOH or a mixture KOH +
332 NaOH), all the FTIR results indicate the OH bands alteration, especially for the 3 inner surface
333 hydroxyls, and the fact that the Al coordination could evolved from octahedral to tetrahedral
334 coordination specifically in the case of the lower crystalline kaolinite (Sanz et al., 1988; Singh
335 and Mackinnon, 1996). We can thus hypothesize that the dissolution is preferentially located at
336 the edge of the particle as well as on the inner OH surface, corroborating the dissolution data
337 obtained before. Indeed, the experimental results are consistent with a dissolution mechanism
338 involving inward movement of a dissolution front from crystal edges and the corner than the
339 surface (Noiriel et al., 2019; Rozalén et al., 2008). During the dissolution, the dissociation of the

340 OH groups could be related to the modification in the Al coordination probably with a change
341 from the octahedral (6-fold, AlO_6) to tetrahedral (4-fold, AlO_4) configurations.

342 By contrast, the spectra of kaolinites treated with NaOH exhibit important changes. Starting from
343 the raw kaolinite spectra, the signal of the OH stretching bands drastically decreases. The region
344 of Si-O modes is totally redefined by the appearance of a single and broad band at 938 cm^{-1} with
345 shoulders at 1001 and 1025 cm^{-1}. Moreover, a broad band at 3400 cm^{-1} and a band at 1650 cm^{-1}
346 appear in the spectra corresponding to the vibrations (stretching and bending respectively) of
347 water. Unfortunately, such signal in the 1100-700 cm^{-1} range is characteristic of the overlaps
348 signal of different mineral phases (*i.e.* zeolite as already highlighted from the XRD profiles plus
349 kaolinite). Consequently, it is difficult to follow the dissolution effect on kaolinite in this range
350 due to (i) the overlapping of zeolite spectra, (ii) the infrared spectra decomposition which is not
351 trivial and (iii) the insufficient sensitive decomposition to observe structural modification.

352 *3.2.2. Change in the Al and Si speciation from XANES*

353 To understand the effects of the alkaline treatment on kaolinites, XANES was undertaken to
354 unravel the evolution of the atomic environment of Si and Al through the dissolution process.
355 Figures 4 and 5 present respectively Al and Si-K-edge XANES measurements obtained on
356 kaolinite samples before and after alkaline treatment at 24h.

357 The Al K-edge spectra (Figure 4) have a similar structural environment corresponding to an
358 isoelectronic AlO_6^{9-} clusters displaying typical features for 1:1 clays with a low site symmetry
359 and Al octahedrally coordinated linked by the edge to form a dioctahedral gibbsitic layer (2/3
360 octahedral sites with Al and a vacancy). The weak shoulder at 1565 eV is assigned to the allowed
361 transition of Al 1s electrons to antibonding t_{tu} state (p-like transition) (Ildefonse et al., 1998; Li et

362 al., 1995). The white line is located at 1570 eV and the peaks located at 1567 eV (before multi-
363 scattering effect) and 1574 eV (post-edge region) may be due to the transitions of Al 1s electrons
364 to t_{2g} and e_g states (d-like transition), respectively. Finally, two broad components also occur in
365 the post-edge region at 1578 eV and 1589 eV due to multi-scattering effect and the first EXAFS
366 oscillation, respectively. According to the alkali treatment effect, the main modification consists
367 in the increase of the component at 1564 eV whatever the treatment used (increasing drastically
368 in the case of NaOH). The Al K-edge energy shift (1569 to 1564 eV) may be directly attributed to
369 the change in coordination number of Al (Ildefonse et al., 1998; Li et al., 1995). The presence of
370 Al(IV) near 1564 eV is evidenced in the case of NaOH or NaOH + KOH treated samples, and
371 finally the Al(VI) at 1569 eV (Figure 4). Note that the presence of Al(V) cannot be excluded as
372 its signal near 1564 eV is combined with that of Al(IV) and Al(VI)[49]. XANES results suggest the
373 presence of Al(IV) after 24h of alkali treatment whatever the treatment used. This fact is clearly
374 evidenced for NaOH treatment and mainly in the case of the KGa-2 sample. However, the
375 resulting spectra in the case of the NaOH treatment (Figure 4) reflects the overlap of zeolite-like
376 mineral with kaolinite one, making difficult to decipher the contribution of one to another to the
377 Al speciation. Indeed, the coordination of Al in zeolite is mainly 4-coordinated (as already
378 observed in the case of the orthoclase mineral) inducing the high amount of Al(IV); it is thus
379 difficult to conclude about the direct effect on Al speciation evolution after 6h (from XRD data)
380 within the kaolinite during NaOH treatment.

381 The Si K-edge spectra of the kaolinite alkali treated (Figure 5) are qualitatively very similar in
382 accordance with the literature (Li et al., 1995). All Si K-edge spectra of kaolinite display a strong
383 edge maximum at 1846 eV which can be ascribed to the 3s transition (Ildefonse et al., 1998). The
384 poorly resolved features 3p and 3d-like transitions at 1849 and 1853 eV is due to the scattering

385 atoms within the tetrahedral layer, and finally the multiple scattering effect (1851 eV) from the
386 more distant shell atoms. No change in the morphology of the spectra is observed. It may be
387 interpreted in a similar way considering that Si present similar structural environment and SiO_4^{4-}
388 clusters. Therefore, regardless of the type of treatment (KOH and NaOH + KOH) no (or very
389 little) modification of the tetrahedral layer of kaolinites is effective. The environmental change in
390 the case of NaOH treatment is related to zeolite precipitation (see before) in which the
391 environment of silicon is modified compared to that of kaolinite.

392 Overall, our XANES measurement at the Si and Al K-edge reveal a strong modification of the Al
393 octahedral layer along the dissolution effect favouring the transformation of Al(VI) into Al(IV or
394 V) regardless of the type of treatment. However, in the case of NaOH treatment, the change in
395 speciation is probably also linked to the precipitation of zeolite (Al speciation being in four-
396 coordinated environment). Moreover, there is no modification related to tetrahedra local
397 organization (tetrahedral layer). Consequently, the latter dissolves with release of Si without
398 modification of its environment.

399 *3.2.3. Quantification of the Al tetracoordinated from 27Al MAS-NMR*

400 To resolve the different Al sites, ^{27}Al MAS NMR experiments and multiple-quantum MAS
401 techniques have been utilized and are reported in Figures 6 and 7 respectively for the two
402 kaolinites, each treatment and for 24h of time. The signal observed at 7.3 and 7.6 ppm for KGa-
403 1b and KGa-2 is consistent with a six-coordinated Al in accordance with the literature
404 (MacKenzie and Smith, 2002) (signal between 10 to +15 ppm). This peak is close to the true
405 isotropic chemical shift (δ_{iso}). The position of this resonance is constant whatever the treatment
406 and the kaolinite used, but it seems that its intensity drastically decreases in the case of NaOH
407 treatment with the increase of Al-four coordinated resonance. For the raw kaolinite, a weak

second peak located at 70.1 and 69.8 ppm for KGa-1b and KGa-2 is attributed to the presence of a four-coordinated Al-O species (MacKenzie and Smith, 2002), and correspond to the presence of accessories mineral, as crandallite in the samples (Chipera and Bish, 2001). This resonance seems to be stable whatever the treatment and time except after 24h. After this period of NaOH + KOH and KOH treatment, a new peak located near 60 ppm is observed and attributed to the presence of four-coordinated Al-O species directly linked to the kaolinite structure. The contribution of the peak (corresponding to the quantification of Al(IV)) represents 1.9 and 12.9 % of the total Al for KGa-1b and KGa-2 after NaOH + KOH treatment, whereas the contribution increases respectively to 8.5 and 14% after KOH treatment.

In the case of NaOH treatment after 24h, ^{27}Al MQMAS NMR experiment was performed to disentangle the contributions from alkali-treated kaolinite, zeolite and crandallite (Figure 7). The decomposition of the signal clearly shows four resonances in the 4-coordinated Al region whatever the type of kaolinite. The peak at about 68 ppm is attributed to crandallite (Kim and Kirkpatrick, 1996). The contribution at 60 ppm is assigned to Al(IV)-coordinated linked to the kaolinite particles and corresponds to 22.7 and 61.7% of Al (IV) for KGa-1b and KGa-2 respectively. Finally, the NMR signals related to the Al(IV) component from zeolites appear at 56 and 58 ppm, corresponding to q^4 Al atoms with only Si neighbors, and a contribution at 63 ppm ascribed to q^3 Al atoms, i.e. with three Si atoms and one neighboring OH group (Dedecek et al., 2012). The investigations realized from NMR analysis clearly evidenced that the alkali treatments induce the change in Al speciation in kaolinite in accordance to XANES experiments: change of Al speciation from (VI) to (IV) but no evidence was done for the presence of Al(V)-coordinated. Moreover, the integration of each contribution shows the importance of (i) kaolinite crystallinity toward dissolution reactivity in alkaline treatment: the KGa-2 being more reactive,

431 inducing the transformation up to 61.7% of Al(IV) after NaOH treatment; and (ii) the role of
432 cation since NaOH treatment is more effective compare to KOH and KOH + NaOH mixtures.

433

434 ### 3.3. Explanation of the dissolution process toward cationic effect in high alkali
435 solution

436 To study more precisely the effect of particle dissolution in various alkaline media, TEM
437 investigations were carried out at the particle scale (Figure 8). Before the alkali treatment, TEM
438 images of both KGa-1b and KGa-2 (Figures 8a and 8e) evidence the recognizable platy and
439 hexagonal crystals of kaolinite. The mean size of the KGa-2 is lower than for KGa-1b, in
440 accordance with the literature (Gormley and Addison, 1983). After 24 h of treatment with 2 M
441 KOH (Figures 8b and 8f), the initial hexagonal shape of kaolinite particles is no more observable
442 whatever the kaolinite samples. Anisotropic dissolution can be observed with apparent higher
443 dissolution of clay minerals crystal edges than basal surfaces (no clear etch pits visible on basal
444 planes or retreat), with a rather homogeneous retreat of all the edges. The retreat of the crystal
445 edges lead to the presence of sub-rounded platy particles instead of the well-shaped platy
446 polyhedron present in the initial material. Affects. This mode of dissolution, with a fastest
447 dissolution of edges (and corners) of the crystal edges, is quite classical as evidenced by local
448 measurements at the mineral surfaces for other types of minerals (*e.g.* on carbonates (Noiriel et
449 al., 2019)). However, due to this dissolution effect, it is almost impossible to determine
450 quantitatively an average length and width of the particles. In the case of 2 M NaOH treatment
451 (Figures 8c and 8g), the dissolution of kaolinite crystals is completely different. Indeed, the
452 overall hexagonal shape of the kaolinite crystals is better preserved, but the dissolution is highly
453 anisotropic, with different dissolution mechanisms from edge to edge with elongated etch pits

454 formed from some crystal edges and all oriented in the same direction, and with a retreat of other
455 edges in a lesser extent. This phenomenon looks like etch pits observed during the dissolution of
456 several silicates like quartz (Brantley et al., 1986) or feldspars (Pollet-Villard et al., 2016) among
457 others. However, even if the formation of etch pits were previously describes on the basal planes
458 of phyllosilicates (Kurganskaya et al., 2012; Kurganskaya and Luttge, 2013), this is the first time
459 that this kind of dissolution process is observed in the case of clay minerals. These oriented
460 dissolutions originate from structural properties of the crystal and could be linked to the
461 activation of defects like dislocations, vacancy sites in octahedral sheets or sites where Al ions
462 could have been substituted by Fe ions (possible substitution about 0.01 Fe atoms per half-cell)
463 and propagation of the dissolution along 2D defects or following chains of weaker bonds into the
464 crystal lattice. The mean length and width of dissolution pits are 192 nm versus 53 nm for KGa-
465 1b and 146 nm versus 36 nm for KGa-2 respectively (±5%). These differences can be explained
466 by the initial size of kaolinite particles inducing differences in term of dissolution pits
467 morphology. In fact, there must be a critical size of dissolution channels. In the case of large
468 particles with good crystallinity, dissolution is slow, and channels can spread over a large surface
469 area along uninterrupted series of bonds in the crystal lattice. On the contrary it is supposed that
470 the smaller and poorly crystalline particles present pits limited in size either because the
471 propagation of the dissolution along a specific defects or chain of bonds will be interrupted by
472 changes in the crystal lattice, or because of the quick coalescence of small pits before they can
473 spread, which lead to a complete dissolution of the external parts of the particles (which is in
474 agreement with the higher dissolution rate observed for KGa-2 kaolinite, see Figure 1 and
475 previous discussions). As a result, the apparent pits sizes for KGa-2 are smaller. With 2M KOH +
476 NaOH treatment (Figures 8d and 8f), a combination of both phenomena is observed, i.e., the
477 hexagonal shape vanishing and the two types of alteration: homogeneous retreat from the edge as

478 observed in KOH treatment, and oriented dissolution from some edges as observed in NaOH
479 treatment. By calculating the number of Al and Si atoms per half kaolinite cell from EDX
480 microanalyses obtained by TEM on discrete kaolinite particles after 24 hours of treatment (Figure
481 9), it is found that there are differences according to the treatments. The evolution is linear, which
482 implies a relationship between the different treatments on kaolinites dissolution without ruling
483 out a different dissolution mode in accordance with TEM photography and dissolution kinetics.
484 Indeed, in the case of a KOH-based treatment, the Al content in the particles decreases with an
485 increase in Si compared to a particle that has not undergone treatment, whereas in the case of
486 NaOH the shift is less significant but results in a decrease in Si with an increase in Al. As
487 expected, the changes induced during the mixed treatment (NaOH + KOH) are intermediate. The
488 fact that both dissolution modes (isotropic and anisotropic) are observed in treatment of kaolinites
489 with KOH + NaOH confirm the effect of the cation (K^+ or Na^+) during the alkali treatment.
490 Finally, in the case of KOH treatment, the isotropic dissolution seems to be more intense at the
491 level of the octahedral layer inducing a decrease in the quantity of Al(VI)-coordinated. In the
492 case of NaOH, the dissolution being oriented, the modifications are less intense since they are
493 located on specific zones. Even if the octahedral layer is destroyed, the tetrahedral layer is also
494 strongly altered, favoring the surface dissolution of kaolinite. For this reason, the amount of Si is
495 lower after a NaOH treatment than after a KOH treatment. Moreover, this type of dissolution
496 probably induces the change in the speciation of Al located at the edge of each oriented
497 dissolution zone.

498 Finally, the dissolution of the octahedral layer acts as an activator for the dissolution of the
499 tetrahedral layer. Consequently, the dissolution of kaolinite seems to be due to the first
500 deprotonation of Al group and thus enhancing negative charges on both Al and Si sites. When the

mechanism is engaged, the dissolution occurs similarly whatever the type of layer. On the other hand, the crystallinity of kaolinite seems to influence the progress of this dissolution. Indeed, in the case of a turbostratic stacking (lower crystallinity; KGa-2) the number of defects and access paths for dissolution is greater, whereas in the case of a kaolinite of good crystallinity, it is more difficult to balance the dissolution process in a congruent manner. According to the literature, the congruence or not of the dissolution of kaolinite is a matter of controversy. Indeed, the potentiometric titration of surface speciation of kaolinite shows that the kaolinite dissolves congruently at pH value < 4 and pH value > 11 (Bauer et al., 1998; Huertas et al., 1998; Pentrák et al., 2009). Moreover, Carroll-Webb and Walther (1988) and Xie and Walther (1992) suggested from calculation and potentiometric titrations that the dissolution is probably nonstoichiometric at first and then followed by a long-term, steady state congruent dissolution then in accordance with this study, whereas Naderi Khorshidi et al. (2018) evidence a congruent dissolution over the time from molecular dynamic. The authors explained that the dissolution mechanism of kaolinite basal surfaces in alkali media as follow: the Na^+ solution triggers more surface hydroxyl groups to dissociate from the octahedral surface than the K^+ solution but in contrast, K^+ solution results in greater dissociation of the aluminate groups than the Na^+ solution. They attributed the different dissolution mechanism of the two cations to their difference in the charge density. Indeed, owing to the smaller size of Na^+ (i.e., higher charge density), Na^+ exhibits stronger interaction with O^- (or OH groups) on the partially deprotonated octahedral surface and therefore, increases the tendency of the dissociation of O^- (or OH groups), not the moieties containing Al atom. Moreover, Carroll-Webb and Walther (1988), through their work on the surface complex reaction model for the pH-dependence of kaolinite dissolution, show that the measure of specific surface area obtained from SEM is smaller than the BET one after dissolution experiments. The authors suggest the presence of small channels (not shown in their paper but suggested) along kaolinite

525 edges which are accessible to Kr adsorption. According to this work and since Na^+ with a higher
526 charge density induced more hydroxyl groups to dissociate than K^+, it is possible to hypothesize
527 that protons or hydroxyl ions can penetrate easily between kaolinite layers starting from these
528 channels inducing an increase of oriented dissolution.

529

530 **4. Conclusion**

531 This study aimed (i) to understand the effect of the alkali treatment onto kaolinites in order to
532 improve their reactivity along alkaline activated materials, and finally to (ii) determine the role of
533 crystal chemistry relative to their reactivities toward alkali activation. Thus, it has been shown
534 that the degree of dissolution of kaolinites (82% of Al released for KGa-2 compare to 75% for
535 KGa-1b in the case of NaOH treatment), is directly related to the type of alkaline treatment and
536 the cation involved. Indeed, the quantity of Si and Al released is relative to the order:
537 KOH<NaOH + KOH<NaOH. This difference can be directly explained by the different charge
538 density between these two cations K^+ or Na^+: the high charge density cation, such as Na^+,
539 induced more dissociation of hydroxyl groups compare to the low charge density cation one (K^+).
540 However, the dissolution rate is higher in the poorly crystallized kaolinites, thus confirming the
541 role of the crystallinity of the samples towards reactivity in an alkaline media. On the other hand,
542 thermodynamic conditions cause zeolite-like precipitation in the case of an alkaline treatment
543 based on NaOH. The dissolution process could thus be considered according to two steps: (i) a
544 first rather short incongruent dissolution corresponding to the activation/dissolution of the
545 octahedral layer by deprotonation (Al being link together to bonding oxygens with Si and to OH
546 groups); (ii) a following congruent dissolution as soon as the system is initiated. This dissolution
547 is accompanied by a change in the speciation of the aluminum probably on the edges of the

548 particles from 6-coordinated to a 4-coordinated one, as shown by XAS and MAS-NMR results.
549 However, the dissolution process at the particle level is different depending on the type of cation
550 used. Indeed, in the case of KOH, the dissolution is homogeneous, starting with the edges and
551 surfaces, whereas in the case of NaOH, the dissolution is probably oriented thanks to areas of less
552 coherence.
553 These new and unique results are essential to better understand the dissolution processes during
554 the first steps of geopolymerization processes but also to better manage the type and reactivity of
555 aluminosilicate alkaline sources and the choice of the cation of the alkaline solution.
556

557 **Acknowledgments**

558 The authors thanks Project INIFUGE supported by Andra under the "Investing in the Future
559 Programme" ("Investissement d'Avenir") - Selected under the Andra Call for Projects:
560 "optimisation of post-dismantling radioactive waste management", organized in cooperation with
561 the French National Research Agency (ANR). Moreover, we acknowledge SOLEIL for provision
562 of synchrotron radiation facilities along project 20180745 and we would like to thank all the
563 members for assistance in using LUCIA beamline, and the French Reǵion Ile de France
564 SESAME program for financial support (700 MHz spectrometer). Finally, the authors thanks B.
565 Terasawa for Cobra, the saturday night fever and 80'ies music for nocturne beamline works.
566

567 **References**

568 Aldabsheh, I., Khoury, H., Wastiels, J., Rahier, H., 2015. Dissolution behavior of Jordanian clay-
569 rich materials in alkaline solutions for alkali activation purpose. Part I. Appl. Clay Sci.
570 115, 238–247. https://doi.org/10.1016/j.clay.2015.08.004
571 Amoureux, J.-P., Fernandez, C., Steuernagel, S., 1996. Z Filtering in MQMAS NMR. J. Magn.
572 Reson. A 123, 116–118. https://doi.org/10.1006/jmra.1996.0221
573 Autef, A., Joussein, E., Gasgnier, G., Pronier, S., Sobrados, I., Sanz, J., Rossignol, S., 2013. Role
574 of metakaolin dehydroxylation in geopolymer synthesis. Powder Technol. 250, 33–39.
575 https://doi.org/10.1016/j.powtec.2013.09.022
576 Bailey, S.W., 1988. Polytypism of 1:1 layer silicates. Hydrous Phyllosilicates Exclus. Micas Rev.
577 Mineral. 19, 9–27.
578 Bauer, A., Berger, G., 1998. Kaolinite and smectite dissolution rate in high molar KOH solutions
579 at 35° and 80°C. Appl. Geochem. 13, 905–916. https://doi.org/10.1016/S0883-
580 2927(98)00018-3
581 Bauer, A., Velde, B., Berger, G., 1998. Kaolinite transformation in high molar KOH solutions.
582 Appl. Geochem. 13, 619–629. https://doi.org/10.1016/S0883-2927(97)00094-2
583 Belver, C., Bañares Muñoz, M.A., Vicente, M.A., 2002. Chemical Activation of a Kaolinite
584 under Acid and Alkaline Conditions. Chem. Mater. 14, 2033–2043.
585 https://doi.org/10.1021/cm0111736
586 Berthonneau, J., Grauby, O., Ferrage, E., Vallet, J.-M., Bromblet, P., Dessandier, D.,
587 Chaudanson, D., Baronnet, A., 2014. Impact of swelling clays on the spalling decay of
588 building limestones: insights from X-ray diffraction profile modeling. Eur. J. Mineral. 26,
589 643–656. https://doi.org/10.1127/0935-1221/2014/0026-2393

590 Brantley, S.L., Crane, S.R., Crerar, D.A., Hellmann, R., Stallard, R., 1986. Dissolution at
591 dislocation etch pits in quartz. Geochim. Cosmochim. Acta 50, 2349–2361.
592 https://doi.org/10.1016/0016-7037(86)90087-6
593 Brindley, G.W., 1986. Relation between Structural Disorder and Other Characteristics of
594 Kaolinites and Dickites. Clays Clay Miner. 34, 239–249.
595 https://doi.org/10.1346/CCMN.1986.0340303
596 Carroll, S.A., Walther, J.V., 1990. Kaolinite dissolution at 25 degrees, 60 degrees, and 80 degrees
597 C. Am. J. Sci. 290, 797–810.
598 Carroll-Webb, S.A., Walther, J.V., 1988. A surface complex reaction model for the pH-
599 dependence of corundum and kaolinite dissolution rates. Geochim. Cosmochim. Acta 52,
600 2609–2623. https://doi.org/10.1016/0016-7037(88)90030-0
601 Catauro, M., Bollino, F., Papale, F., Lamanna, G., 2014. Investigation of the sample preparation
602 and curing treatment effects on mechanical properties and bioactivity of silica rich
603 metakaolin geopolymer. Mater. Sci. Eng. C 36, 20–24.
604 https://doi.org/10.1016/j.msec.2013.11.026
605 Chipera, S.J., Bish, D.L., 2001. Baseline Studies of the Clay Minerals Society Source Clays:
606 Powder X-ray Diffraction Analyses. Clays Clay Miner. 49, 398–409.
607 https://doi.org/10.1346/CCMN.2001.0490507
608 Costanzo, P.A., Guggenheim, S., 2001. Baseline studies of the clay minerals society source clays:
609 preface. Clays Clay Miner. 49, 371–371.
610 Cui, X.-M., Zheng, G.-J., Han, Y.-C., Su, F., Zhou, J., 2008. A study on electrical conductivity of
611 chemosynthetic Al_2O_3–$2SiO_2$ geoploymer materials. J. Power Sources, Selected papers
612 from the International Battery Materials Association 2007 Conference. In Memoriam of
613 Juergen Besenhard 184, 652–656. https://doi.org/10.1016/j.jpowsour.2008.03.021

614 Dedecek, J., Balgová, V., Pashkova, V., Klein, P., Wichterlová, B., 2012. Synthesis of ZSM-5
615 Zeolites with Defined Distribution of Al Atoms in the Framework and Multinuclear MAS
616 NMR Analysis of the Control of Al Distribution. Chem. Mater. 24, 3231–3239.
617 https://doi.org/10.1021/cm301629a
618 Duxson, P., Fernández-Jiménez, A., Provis, J.L., Lukey, G.C., Palomo, A., van Deventer, J.S.J.,
619 2007. Geopolymer technology: the current state of the art. J. Mater. Sci. 42, 2917–2933.
620 https://doi.org/10.1007/s10853-006-0637-z
621 Farmer, V.C., Fraser, A.R., Tait, J.M., 1979. Characterization of the chemical structures of
622 natural and synthetic aluminosilicate gels and sols by infrared spectroscopy. Geochim.
623 Cosmochim. Acta 43, 1417–1420. https://doi.org/10.1016/0016-7037(79)90135-2
624 Farmer, V.C., Russell, J.D., 1964. The infra-red spectra of layer silicates. Spectrochim. Acta 20,
625 1149–1173. https://doi.org/10.1016/0371-1951(64)80165-X
626 Gormley, I.P., Addison, J., 1983. The in Vitro cytotoxicity of some standard clay mineral dusts in
627 the respirable size range. Clay Miner. 18, 153–163.
628 https://doi.org/10.1180/claymin.1983.018.2.04
629 Habert, G., d'Espinose de Lacaillerie, J.B., Roussel, N., 2011. An environmental evaluation of
630 geopolymer based concrete production: reviewing current research trends. J. Clean. Prod.
631 19, 1229–1238. https://doi.org/10.1016/j.jclepro.2011.03.012
632 Heller-Kallai, L., Lapides, I., 2007. Reactions of kaolinites and metakaolinites with NaOH—
633 comparison of different samples (Part 1). Appl. Clay Sci. 35, 99–107.
634 https://doi.org/10.1016/j.clay.2006.06.006
635 Huertas, F.J., Chou, L., Wollast, R., 1999. Mechanism of kaolinite dissolution at room
636 temperature and pressure Part II: kinetic study. Geochim. Cosmochim. Acta 63, 3261–
637 3275. https://doi.org/10.1016/S0016-7037(99)00249-5

638 Huertas, F.J., Chou, L., Wollast, R., 1998. Mechanism of Kaolinite Dissolution at Room
639 Temperature and Pressure: Part 1. Surface Speciation. Geochim. Cosmochim. Acta 62,
640 417–431. https://doi.org/10.1016/S0016-7037(97)00366-9
641 Ildefonse, P., Cabaret, D., Sainctavit, P., Calas, G., Flank, A.-M., Lagarde, P., 1998. Aluminium
642 X-ray absorption Near Edge Structure in model compounds and Earth's surface minerals.
643 Phys. Chem. Miner. 25, 112–121. https://doi.org/10.1007/s002690050093
644 Johnston, C.T., Agnew, S.F., Bish, D.L., 1990. Polarized Single-Crystal Fourier-Transform
645 Infrared Microscopy of Ouray Dickite and Keokuk Kaolinite. Clays Clay Miner. 38, 573–
646 583. https://doi.org/10.1346/CCMN.1990.0380602
647 Kim, Y., Kirkpatrick, R.J., 1996. Application of MAS NMR spectroscopy to poorly crystalline
648 minerals: viséite. Mineral. Mag. 60, 957–962.
649 https://doi.org/10.1180/minmag.1996.060.403.10
650 Kuenzel, C., Neville, T.P., Donatello, S., Vandeperre, L., Boccaccini, A.R., Cheeseman, C.R.,
651 2013. Influence of metakaolin characteristics on the mechanical properties of geopolymers.
652 Appl. Clay Sci. 83–84, 308–314. https://doi.org/10.1016/j.clay.2013.08.023
653 Kurganskaya, I., Arvidson, R.S., Fischer, C., Luttge, A., 2012. Does the stepwave model predict
654 mica dissolution kinetics? Geochim. Cosmochim. Acta 97, 120–130.
655 https://doi.org/10.1016/j.gca.2012.08.033
656 Kurganskaya, I., Luttge, A., 2013. A comprehensive stochastic model of phyllosilicate
657 dissolution: Structure and kinematics of etch pits formed on muscovite basal face.
658 Geochim. Cosmochim. Acta 120, 545–560. https://doi.org/10.1016/j.gca.2013.06.038
659 Li, D., Bancroft, G.M., Fleet, M.E., Feng, X.H., Pan, Y., 1995. Al K-edge XANES spectra of
660 aluminosilicate minerals. Am. Mineral. 80, 432–440. https://doi.org/10.2138/am-1995-5-
661 602

662 Lin, D.-C., Xu, X.-W., Zuo, F., Long, Y.-C., 2004. Crystallization of JBW, CAN, SOD and ABW
663 type zeolite from transformation of meta-kaolin. Microporous Mesoporous Mater. 70, 63–
664 70. https://doi.org/10.1016/j.micromeso.2004.03.003
665 MacKenzie, K.J.D., Smith, M.E., 2002. Multinuclear Solid-State Nuclear Magnetic Resonance of
666 Inorganic Materials. Elsevier.
667 Massiot, D., Fayon, F., Capron, M., King, I., Calvé, S.L., Alonso, B., Durand, J.-O., Bujoli, B.,
668 Gan, Z., Hoatson, G., 2002. Modelling one- and two-dimensional solid-state NMR spectra.
669 Magn. Reson. Chem. 40, 70–76. https://doi.org/10.1002/mrc.984
670 Medek, A., Harwood, J.S., Frydman, L., 1995. Multiple-Quantum Magic-Angle Spinning NMR:
671 A New Method for the Study of Quadrupolar Nuclei in Solids. J. Am. Chem. Soc. 117,
672 12779–12787. https://doi.org/10.1021/ja00156a015
673 Medri, V., Fabbri, S., Ruffini, A., Dedecek, J., Vaccari, A., 2011. SiC-based refractory paints
674 prepared with alkali aluminosilicate binders. J. Eur. Ceram. Soc. 31, 2155–2165.
675 https://doi.org/10.1016/j.jeurceramsoc.2011.05.006
676 Murray, H.H., 2006. Applied clay mineralogy: occurrences, processing, and applications of
677 kaolins, bentonites, palygorskite, sepiolite, and common clays. Elsevier.
678 Murray, H.H., 2000. Traditional and new applications for kaolin, smectite, and palygorskite: a
679 general overview. Appl. Clay Sci. 17, 207–221.
680 Naderi Khorshidi, Z., Tan, X., Liu, Q., Choi, P., 2018. Molecular dynamics study of the
681 dissolution mechanism of kaolinite basal surfaces in alkali media. Appl. Clay Sci. 152, 29–
682 37. https://doi.org/10.1016/j.clay.2017.10.025
683 Naderi Khorshidi, Z., Tan, X., Liu, Q., Choi, P., 2017. Influence of structural Al and Si vacancies
684 on the interaction of kaolinite basal surfaces with alkali cations: A molecular dynamics

685 study. Comput. Mater. Sci. 140, 267–274.
686 https://doi.org/10.1016/j.commatsci.2017.09.004
687 Noiriel, C., Oursin, M., Saldi, G., Haberthür, D., 2019. Direct Determination of Dissolution Rates
688 at Crystal Surfaces Using 3D X-ray Microtomography. ACS Earth Space Chem. 3, 100–
689 108. https://doi.org/10.1021/acsearthspacechem.8b00143
690 Panagiotopoulou, Ch., Kontori, E., Perraki, Th., Kakali, G., 2007. Dissolution of aluminosilicate
691 minerals and by-products in alkaline media. J. Mater. Sci. 42, 2967–2973.
692 https://doi.org/10.1007/s10853-006-0531-8
693 Papulovskiy, E., Shubin, A.A., Terskikh, V.V., Pickard, C.J., Lapina, O.B., 2013. Theoretical and
694 experimental insights into applicability of solid-state ^{93}Nb NMR in catalysis. Phys. Chem.
695 Chem. Phys. 15, 5115–5131. https://doi.org/10.1039/C3CP44016H
696 Pentrák, M., Madejová, J., Komadel, P., 2009. Acid and alkali treatment of kaolins. Clay Miner.
697 44, 511–523. https://doi.org/10.1180/claymin.2009.044.4.511
698 Plançon, A., Giese, R.F., Synderf, R., 1988. The Hinckley index for kaolinites. Clay Miner. 23,
699 249–260.
700 Pollet-Villard, M., Daval, D., Fritz, B., Knauss, K.G., Schäfer, G., Ackerer, P., 2016. Influence of
701 etch pit development on the surface area and dissolution kinetics of the orthoclase (001)
702 surface. Chem. Geol. 447, 79–92. https://doi.org/10.1016/j.chemgeo.2016.09.038
703 Rahier, H., Simons, W., Mele, B.V., Biesemans, M., 1997. Low-temperature synthesized
704 aluminosilicate glasses. J. Mater. Sci. 11.
705 Ravel, B., Newville, M., 2005. ATHENA and ARTEMIS: interactive graphical data analysis
706 using IFEFFIT. Phys. Scr. 2005, 1007. https://doi.org/10.1238/Physica.Topical.115a01007

Rouxhet, P.G., Samudacheata, N., Jacobs, H., Anton, O., 1977. Attribution of the OH stretching bands of kaolinite. Clay Miner. 12, 171–179. https://doi.org/10.1180/claymin.1977.012.02.07

Rozalén, M.L., Huertas, F.J., Brady, P.V., Cama, J., García-Palma, S., Linares, J., 2008. Experimental study of the effect of pH on the kinetics of montmorillonite dissolution at 25°C. Geochim. Cosmochim. Acta 72, 4224–4253. https://doi.org/10.1016/j.gca.2008.05.065

Sakharov, B.A., Drits, V.A., McCarty, D.K., Walker, G.M., 2016. Modeling powder x-ray diffraction patterns of the clay minerals society kaolinite standards: KGa-1, KGa-1b, and KGa-2. Clays Clay Miner. 64, 314–333. https://doi.org/10.1346/CCMN.2016.0640307

San Nicolas, R., Cyr, M., Escadeillas, G., 2013. Characteristics and applications of flash metakaolins. Appl. Clay Sci. 83–84, 253–262. https://doi.org/10.1016/j.clay.2013.08.036

Sanz, J., Madani, A., Serratosa, J.M., Moya, J.S., Aza, S., 1988. Aluminum-27 and Silicon-29 Magic-Angle Spinning Nuclear Magnetic Resonance Study of the Kaolinite-Mullite Transformation. J. Am. Ceram. Soc. 71, C418–C421. https://doi.org/10.1111/j.1151-2916.1988.tb07513.x

Sieber, W., Meier, W.M., 1974. Formation and Properties of Losod, a New Sodium Zeolite. Helv. Chim. Acta 57, 1533–1549. https://doi.org/10.1002/hlca.19740570608

Singer, Arieh., Berkgaut, Vadim., 1995. Cation Exchange Properties of Hydrothermally Treated Coal Fly Ash. Environ. Sci. Technol. 29, 1748–1753. https://doi.org/10.1021/es00007a009

Singh, B., Mackinnon, I.D.R., 1996. Experimental Transformation of Kaolinite to Halloysite. Clays Clay Miner. 44, 825–834. https://doi.org/10.1346/CCMN.1996.0440614

van Deventer, J.S.J., Provis, J.L., Duxson, P., Lukey, G.C., 2007. Reaction mechanisms in the geopolymeric conversion of inorganic waste to useful products. J. Hazard. Mater., First

731 International Conference on Engineering for Waste Treatment: Beneficial Use of Waste
732 and By-Products (WasteEng2005) 139, 506–513.
733 https://doi.org/10.1016/j.jhazmat.2006.02.044
734 Xie, Z., Walther, J.V., 1992. Incongruent dissolution and surface area of kaolinite. Geochim.
735 Cosmochim. Acta 56, 3357–3363. https://doi.org/10.1016/0016-7037(92)90383-T
736 Xu, H., van Deventer, J.S.J., 2003. The effect of alkali metals on the formation of geopolymeric
737 gels from alkali-feldspars. Colloids Surf. Physicochem. Eng. Asp. 216, 27–44.
738 https://doi.org/10.1016/S0927-7757(02)00499-5
739 Xu, H., Van Deventer, J.S.J., 2000. The geopolymerisation of alumino-silicate minerals. Int. J.
740 Miner. Process. 59, 247–266. https://doi.org/10.1016/S0301-7516(99)00074-5
741

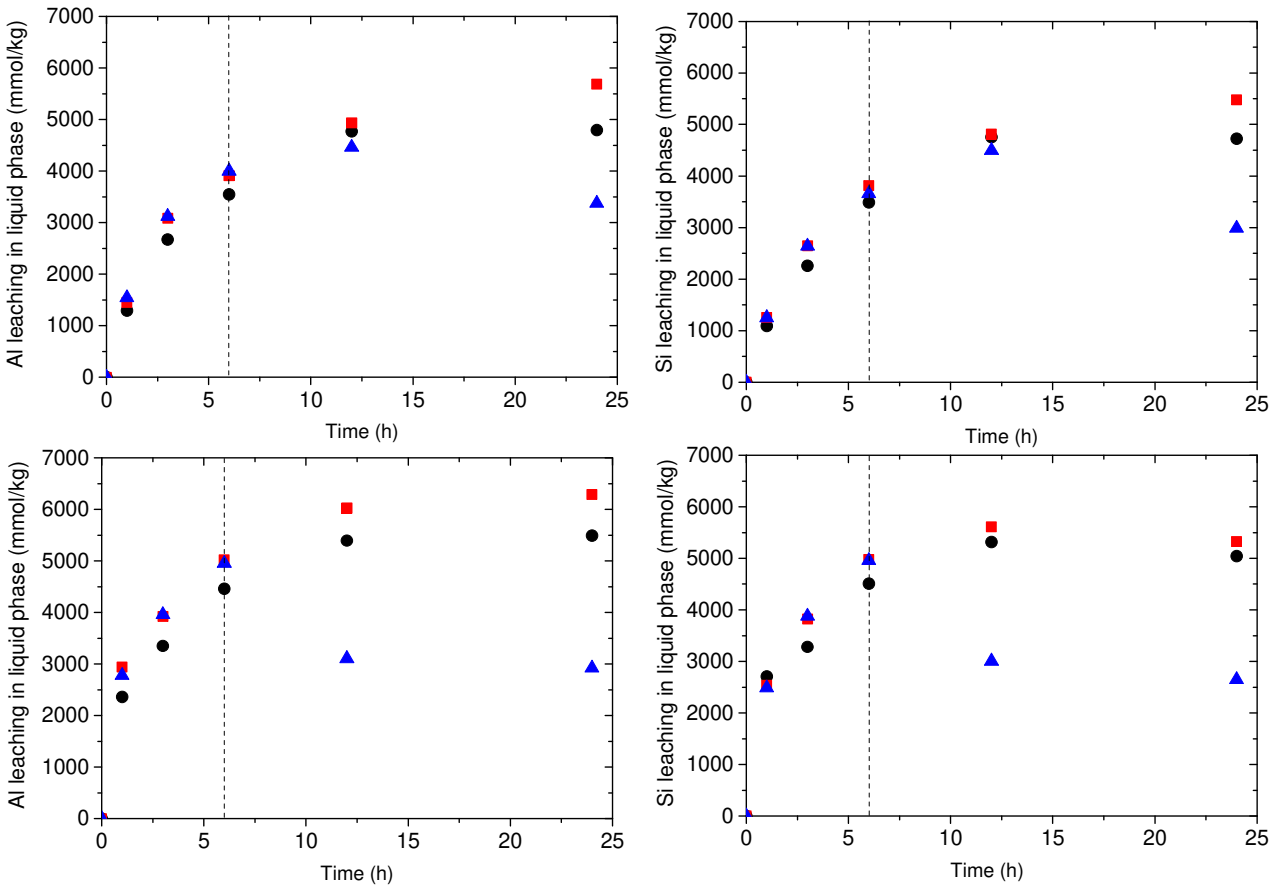

Figure 1. Proportion of Al (left) and Si (right) released (in mmol/kg of initial kaolinite) from kaolinites KGa-1b (upper diagrams) and KGa-2 (bottom diagrams) after various 2M alkali treatment along time (1, 3, 6, 12 and 24h). Circle, triangle and square refer to alkali treatments as KOH, NaOH and KOH + NaOH mixture, respectively. The dash line corresponds to the beginning of precipitation (6h).

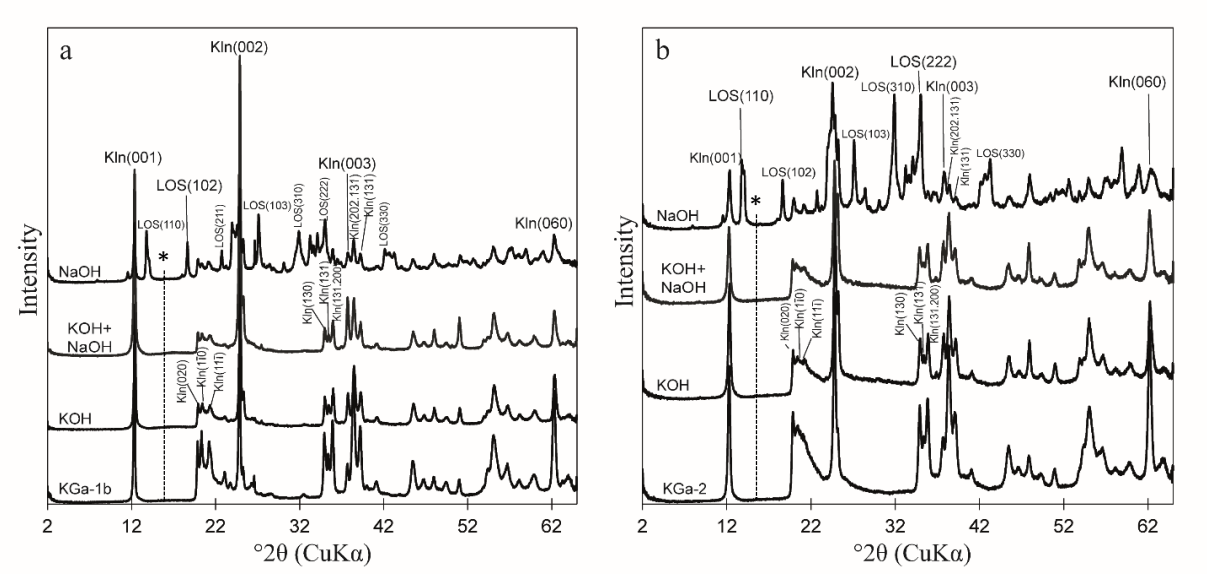

Figure 2. X-ray diffraction patterns of KGa-1b (a) and KGa-2 (b) after 24h of 2 M alkali treatment (KOH, NaOH and KOH + NaOH mixture). Kln and LOS refer to kaolinite and Losod-like zeolite, respectively, and * to crandallite.

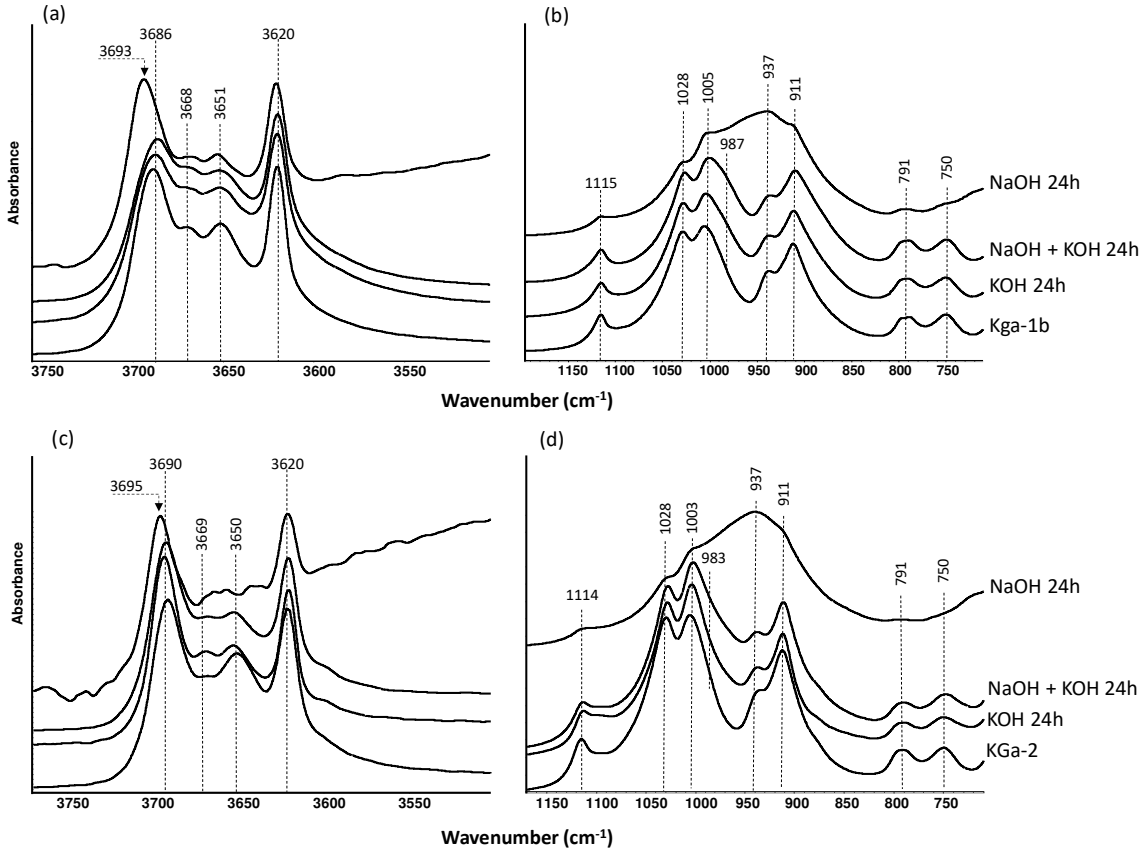

Figure 3. FTIR spectra of KGa-1b (a, b) and KGa-2 (c, d) after 24h of 2M alkali treatment (KOH, NaOH and KOH + NaOH mixture). Curves have been translated for the sake of clarity.

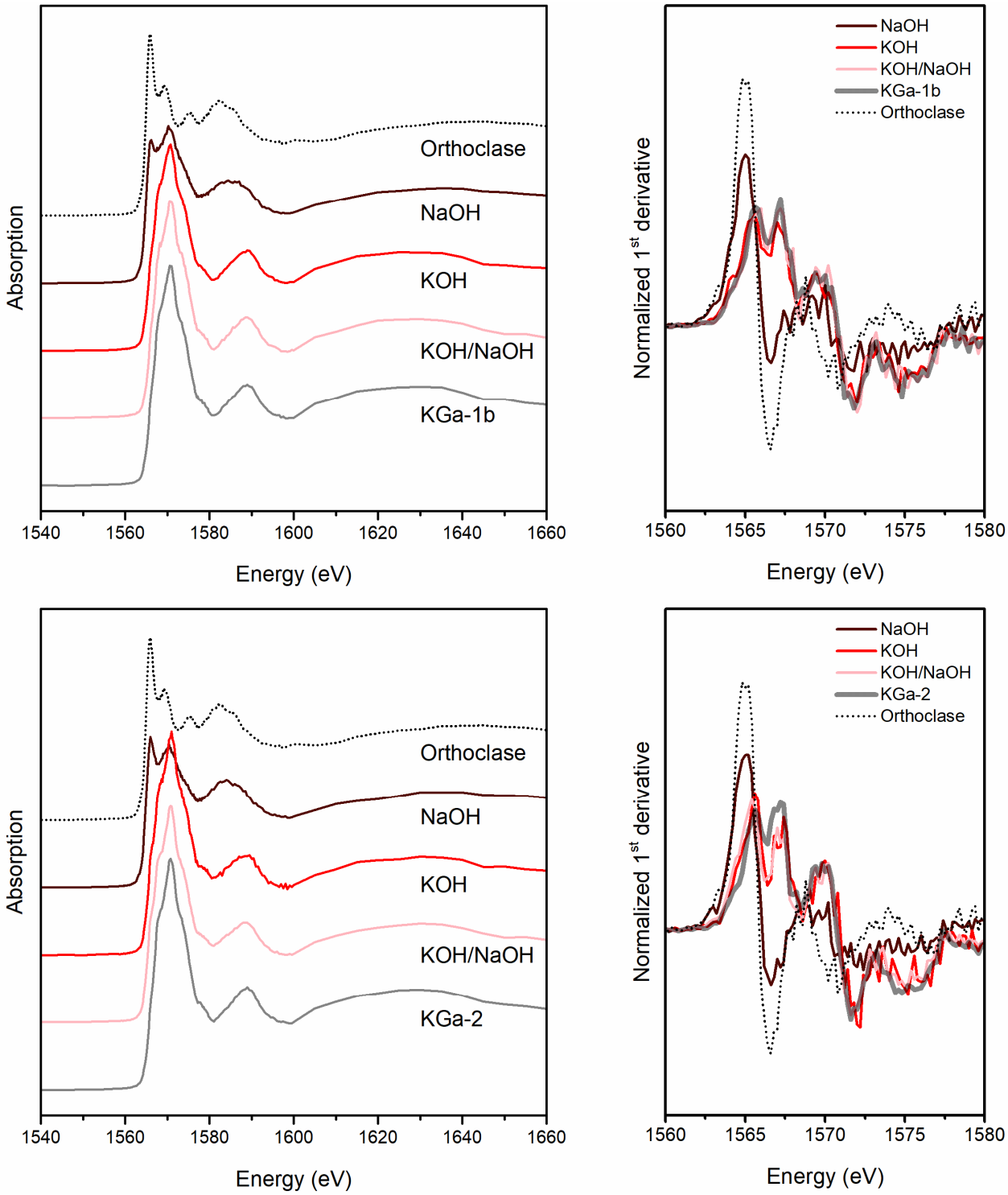

Figure 4. XANES and first derivative spectra at the Al K-edge of KGa-1b (top) and KGa-2 (bottom) raw samples and after 24h of 2M of KOH, NaOH and KOH + NaOH alkali treatment. An offset was applied along the y-axis to all XANES curves for clarity.

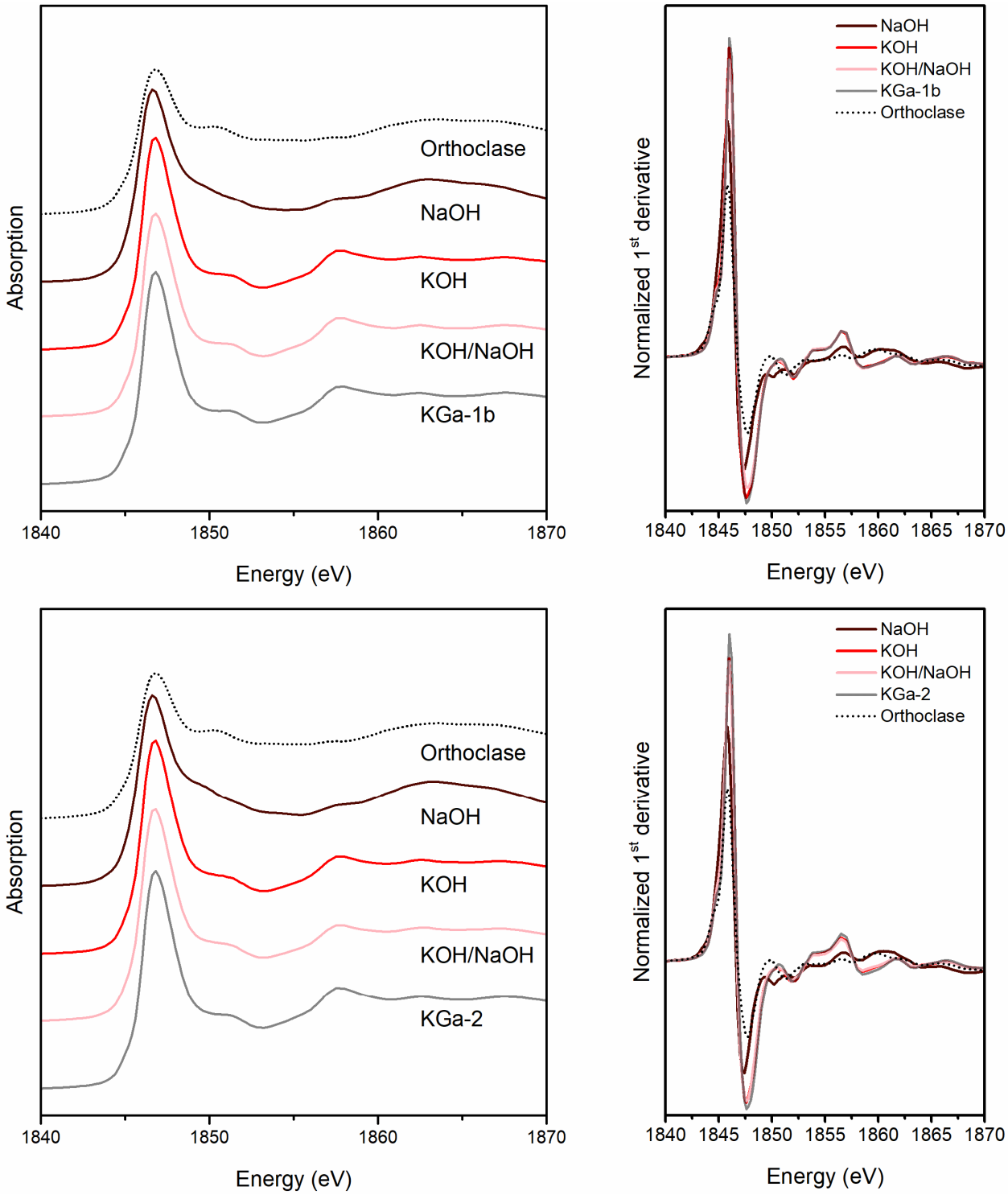

Figure 5. XANES and first derivatives spectra at the Si K-edge of KGa-1b (top) and KGa-2 (bottom) raw samples and after 24h of 2M of KOH, NaOH and KOH + NaOH alkali treatment. An offset was applied along the y-axis to all XANES curves for clarity.

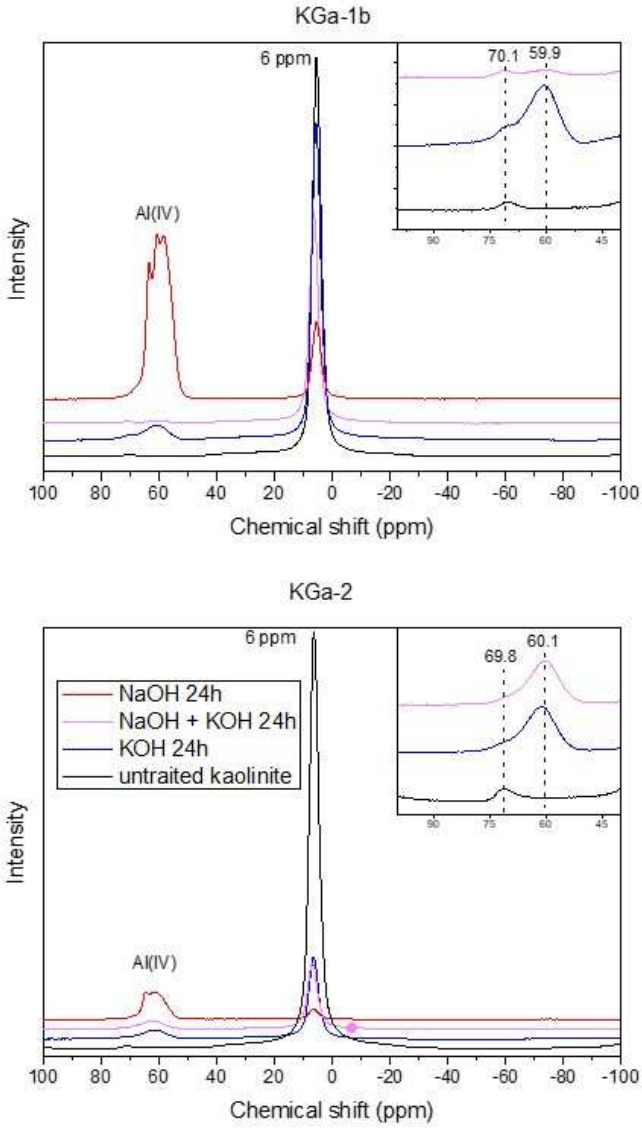

Figure 6. ^{27}Al MAS NMR spectra of KGa-1b (top) and KGa-2 (bottom) samples after 24h of KOH, KOH + NaOH and NaOH treatments, and zoom in the region 45 to 80 ppm.

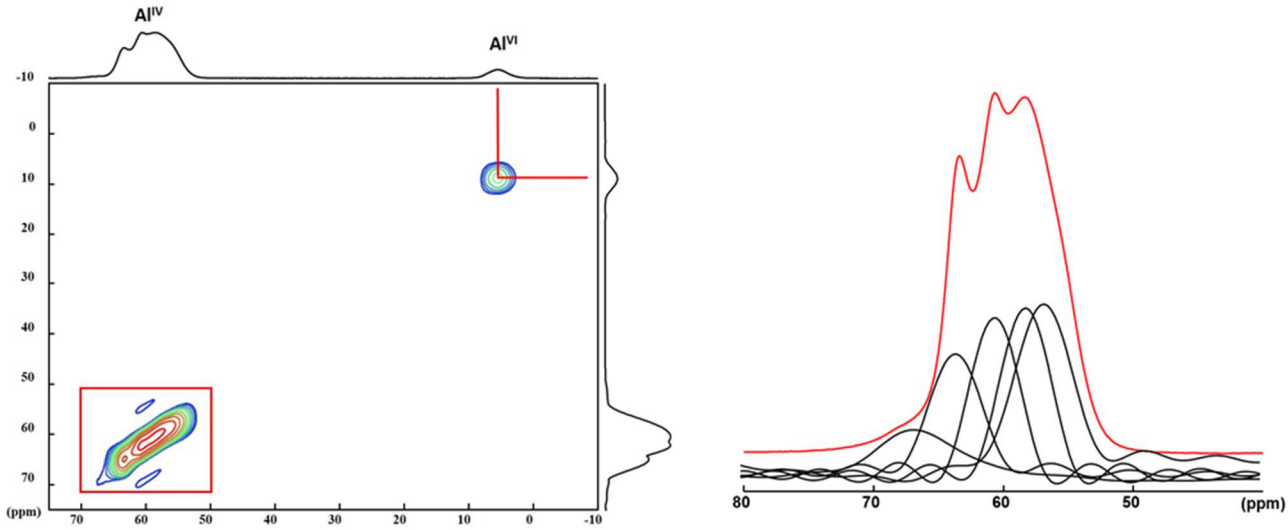

Figure 7. Example of ^{27}Al MQMAS spectrum of KGa-1b after 24h of NaOH treatment (left), MAS spectrum (in red) and MQMAS isotropic projections (in black) in the right hand.

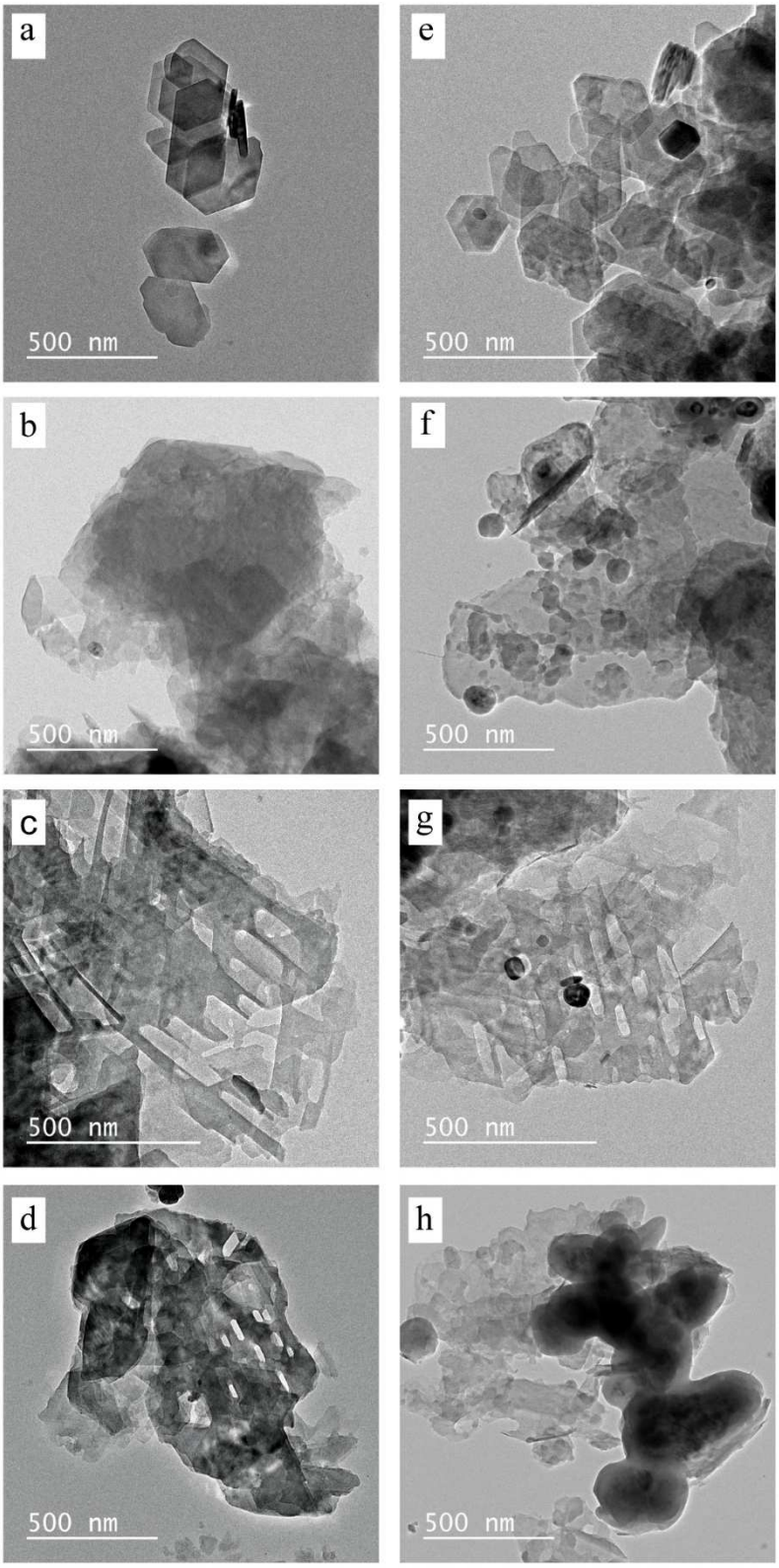

Figure 8. TEM images of KGa-1b (left column) and KGa-2 (right column) samples before (a, e) and after 24h of 2 M of KOH (b, f), NaOH (c, g) and KOH + NaOH (d, h) alkali treatments.

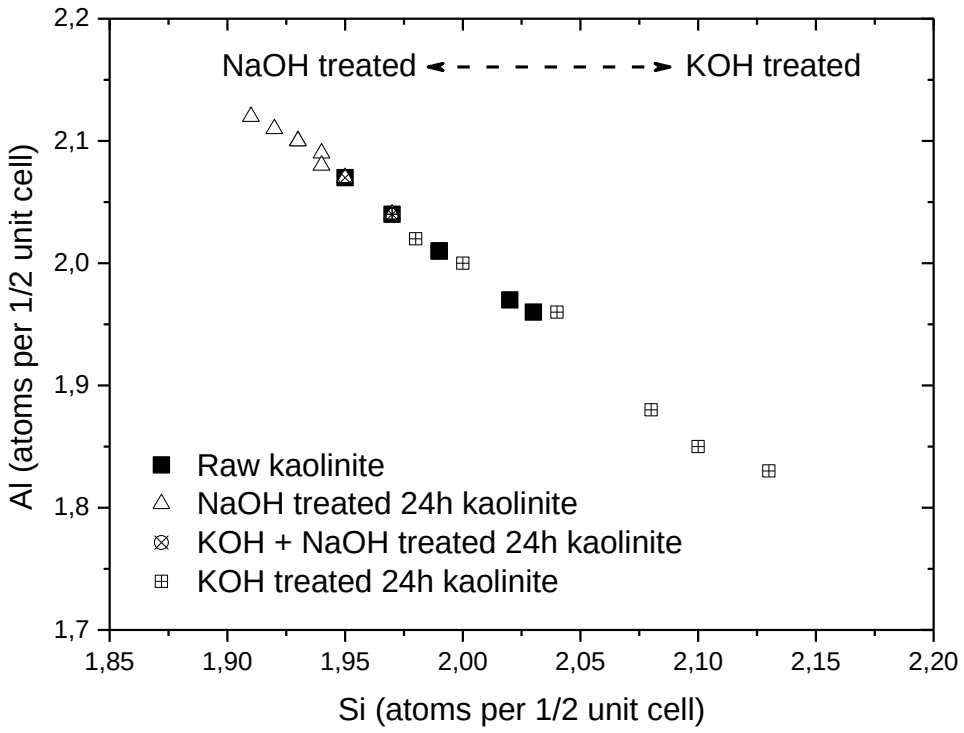

Figure 9. Evolution of the number of Al and Si atoms per half kaolinite unit-cell from EDX microanalyses obtained by TEM on discrete kaolinite KGa-1b and KGa-2 particles after 24 hours of treatment.

Alkali treatment of kaolinite

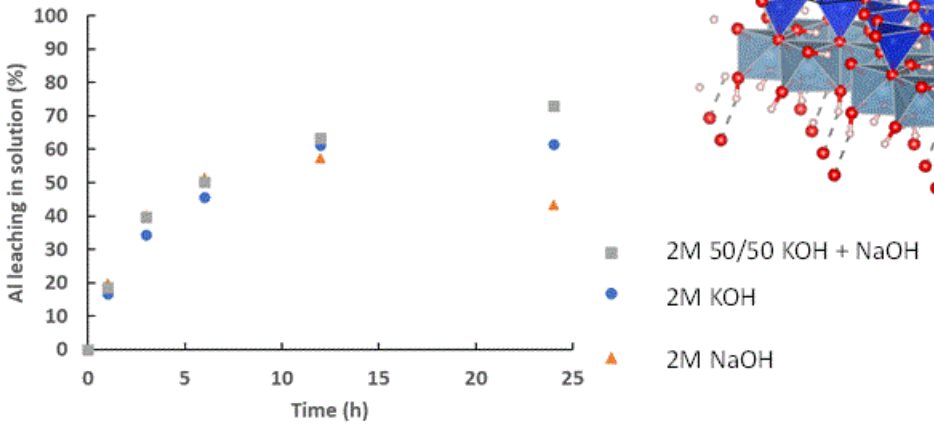

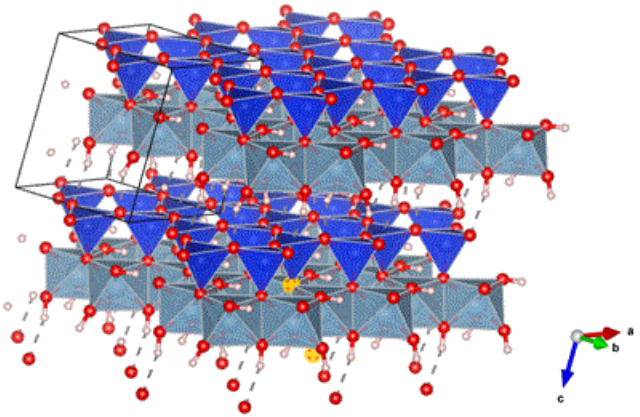

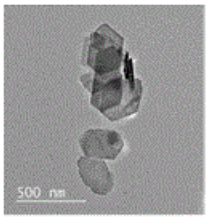

KOH

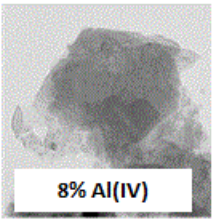

Increasing reactivity

NaOH

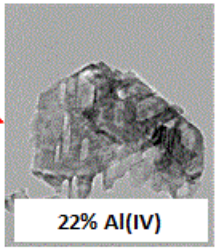

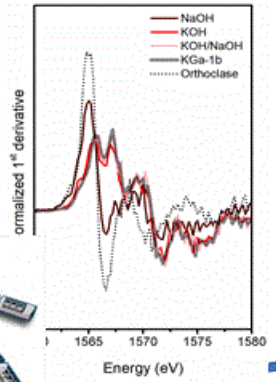

Cationic effect